PNAS
www.pnas.org

Supplementary Information for

Rbm24 controls poly(A) tail length and translation efficiency of *crystallin* mRNAs in the lens via cytoplasmic polyadenylation

Ming Shao, Tong Lu, Chong Zhang, Yi-Zhuang Zhang, Shu-Hui Kong, and De-Li Shi

Ming Shao and De-Li Shi
Email: shaoming@sdu.edu.cn; de-li.shi@upmc.fr

This PDF file includes:

Supplementary text
Figures S1 to S9
Legends for Movies S1 to S3
Legends for Datasets S1 to S6
SI References

Other supplementary materials for this manuscript include the following:

Movies S1 to S3
Datasets S1 to S6

www.pnas.org/cgi/doi/10.1073/pnas.1917922117

Supplementary Information Text

Materials and Methods

Ethical statement

All experiments were performed according to the ARRIVE guidelines issued by the Ethics Committee for Animal Research of Life Science of Shandong University (permit number SYDWLL-2018-05).

Zebrafish embryos

Embryos were cultured at 28.5°C in a temperature-controlled incubator. Microinjections were performed at 1- to 4-cell stage using a PLI-100A Picoliter Microinjector (Warner Instruments). To reduce pigment development in some experiments, embryos were cultured in the presence of 0.003% (w/v) phenylthiourea (Sigma-Aldrich) from 10 hpf onward. Dissections of larval stage embryos were performed under anesthesia in tricaine solution (0.17 $mgmL^{-1}$).

Generation of *rbm24a* mutant and transgenic lines

TALEN (transcription activator-like effector nuclease) repeat variable di-residues recognizing DNA sequences within the first exon of *rbm24a* gene were engineered through the Golden Gate Assembly method (1), using the Golden Gate TALEN and TAL Effector Kit (#1000000016) from Addgene. The constructs were assembled in the modified pCS2+KKR and pCS2+ELD vectors (2). The two TALEN mRNAs (200 pg each) were injected into 1-cell stage embryo, and positive targeting effects were determined by sequencing PCR products amplified using pooled genomic DNA from 15 randomly selected embryos at 24 hpf as templates. The remaining embryos were reared to adulthood for outcrosses to screen F1 offspring using genomic DNA extracted from tail fins (3).

All transgenes were cloned by Gibson ligation in the Tol2 vector between the minimal *cis*-sequences of *Tol2* transposon element (4). To generate the *Tg(cmlc2:rbm24a-2a-GFP)* transgene, *rbm24a* and *GFP* coding regions, which were separated by the coding sequence for a p2A peptide, were fused with a *cmlc2* (*cardiac myosin light chain 2*) promoter region (5). The *Tg(cryaa:rbm24a-GFP)* and *Tg(cryaa:rbm24aΔRRM-GFP)* transgenes were created by fusion of *rbm24a-GFP* or *rbm24aΔRRM-GFP* coding sequence with a *cryaa* promoter region (-977 to +101 bp). To obtain the *Tg(cryaa:GFP)* transgenic line, GFP coding region was ligated between the ß-globin leader sequence and the SV-40 ploy(A) signal, and placed under the control of the *cryaa* promoter region. To construct the *Tg(cryaa:crygm2d1-GFP)* transgene, the complete exonic and intronic sequences of *crygm2d1* gene were fused with the *cryaa* promoter, and the GFP coding sequence was inserted into the coding region of the third exon, before the stop codon. The plasmid was injected into 1-cell stage embryos (10 pg/embryo), along with synthetic mRNAs encoding Tol2 transposase (100 pg/embryo). Transgenic embryos or adult fish were screened by examination of tissue-specific fluorescence.

Expression constructs and synthetic mRNAs for microinjection

The coding sequences of zebrafish *pabpc1l*, *cpeb1b* and *rbm24a* were cloned in pCS2 vector inframe with the 6 myc epitopes or the GFP sequence via Gibson ligation. Deletions of the

sequences coding for *rbm24a* N-terminal region (*rbm24aΔRRM*) or C-terminal region (*rbm24aΔC*) were generated by PCR. The vectors were linearized with *Not* I, and capped synthetic mRNAs were transcribed using mMESSAGE mMACHINE SP6 kit (Invitrogen).

Parabiosis experiments

At 1-cell stage, *rbm24a* mutant embryos were labeled with RLDx (rhodamine-lysine dextran). At sphere stage, a WT embryo and a labeled *rbm24a* mutant embryo were manually dechorionated in an agar-coated Petri dish containing 1 x Ringer's buffer supplemented with penicillin-streptomycin, and a small lesion was surgically created at the animal pole region. The two embryos were joined together by apposing and pressing the wound regions. The parabiotic pairs were then placed in a glass culture dish in 1/3 x Ringer's buffer supplemented with antibiotics, and allowed to develop until they reached appropriate stages.

Generation of chimeric embryos by cell transplantation

This was performed using the protocol and appropriate cell lineage tracers as described previously (6-8). Briefly, WT or mutant embryos were first labeled with FLDx (fluorescein-lysine dextran) or RFP by injecting the dye or the corresponding mRNAs at 1-cell stage. At sphere stage, a small group of cells in the blastodisc were aspirated using the PLI-100A Pneumatic Microinjector, and transplanted into the animal pole region of unlabeled stage-matched recipients. At 1 dpf, chimeric embryos with fluorescent cells essentially in the lens were selected for further analysis.

RNA library preparation and RNA-seq

Total RNAs were extracted from embryos at 33 hpf using TRIzol reagent (Invitrogen), and were precipitated by 50% (v/v) isopropanol in the presence of glycogen (20 μg) as carrier. Polyadenylated mRNAs were captured by the poly(A) mRNA Magnetic Isolation Module (NEB). The mRNA libraries were constructed using NEBNext Ultra RNA Library Prep Kit for Illumina. Specifically, mRNA fragmentation and priming were performed using NEBNext First Strand Synthesis Reaction Buffer and NEBNext Random Primers. First and second strand cDNAs were synthesized using ProtoScript II Reverse Transcriptase and Second Strand Synthesis Enzyme Mix, respectively. After purification by AxyPrep Mag PCR Clean-up (Axygen), double-stranded cDNAs were treated with End Prep Enzyme Mix to repair both ends, followed by dA-tailing and ligation of adaptors. Size selection of adaptor-ligated cDNAs was performed using AxyPrep Mag PCR Clean-up (Axygen), and fragments with an average insert size of 300 bp were recovered. Each library was then amplified by PCR for 11 cycles, and 150 bp paired-end sequencing was performed on Illumina HiSeq 2000 to get the raw data (9). The quality was controlled using Cutadapt (10) and FastQC (Johns Hopkins University). Sequencing results obtained from three independent samples were assembled and aligned using StringTi (Johns Hopkins University). Differential expression was analyzed using DESeq2 (11) and edgeR (12). Volcano scatter plots were generated using GraphPad Prism 6. Analysis of alternative

splicing events was performed using ASprofile (13), which takes a GTF transcript file created by Cufflinks (14) as input.

RNA immunoprecipitation and qPCR (RIP-qPCR)

Two hundreds of *Tg(cryaa:rbm24a-GFP)* or *Tg(cryaa:rbm24aΔRRM-GFP)* transgenic embryos at 2 dpf were crosslinked in 0.9 mL formaldehyde (1%) for 10 minutes at room temperature, and then quenched by adding 0.3 mL glycine (1 M). Following two washes in ice-cold PBS, the embryos were transferred to 1 mL RIPA buffer (20 mM Tris-HCl, pH 7.5, 150 mM NaCl, 1 mM EDTA, 1 mM EGTA, 1% NP-40) supplemented with RNasin and protease inhibitors, and homogenized under ice-cold water bath by sonication at 30 watts for 6 cycles of 18 seconds with an interval of 92 seconds, using a JY92-IIN Ultrasonic Homogenizer (Ningbo Scientz Biotechnology Co., Ltd). The lysate was cleared by centrifugation at 12,000 *g* for 10 minutes, and 100 µL of the supernatant was saved as input control. The remaining supernatant was pre-absorbed by incubation with 40 µL protein G Dynabeads (10004D, Novex) on a rotary shaker at 4 °C for 1 hour. Anti-GFP antibody (11814460001, Roche Diagnostics) or anti-myc antibody (ab32, Abcam) conjugated protein G Dynabeads were prepared in advance by incubation of the beads (80 µL) with 3.2 µg of the antibody at 4 °C overnight, followed by several washes in RIPA buffer. The lysate was divided into two equal parts and mixed with 20 µL anti-GFP antibody conjugated beads as IP+ sample or anti-myc antibody conjugated beads as IP- control sample. Following incubation on a rotary shaker at 4°C overnight, the beads were separated on a magnetic stand and rinsed with 1 mL ice-cold wash buffer (50 mM Tris-HCl, pH 7.5, 1% NP-40, 1% sodium deoxycholate, 0.1% SDS, 1 mM EDTA, 1 M NaCl, 2 M urea, 0.2 mM PMSF) for 6 times at room temperature. The RNPs on the beads and the input control were simultaneously decrosslinked by incubation in 100 µL elute buffer (50 mM Tris-HCl, pH 7.5, 5 mM EDTA, 10 mM DTT, 1% SDS) at 70°C for 45 minutes. The samples were extracted by adding 300 µL TRIzol reagent and 80 µL chloroform, and RNAs were precipitated using an equal volume of isopropanol and 0.5 M ammonium acetate, with glycogen (20 µg) as carrier. Following digestion of genomic DNA by DNase I treatment, purified RNAs were reverse transcribed using random primers, and the cDNAs were analyzed by qPCR using gene-specific primers (Dataset S6).

Poly(A) tail-length assay

Total RNAs were prepared from WT embryos and *rbm24a* mutants at 33 hpf. Poly(G/I) tailing and reverse transcription were performed using the Poly(A)-Tail Length Assay kit according to manufacturer's recommendation (ThermoFischer). Poly(A) tail PCR was performed using the universal reverse primer and one or two (nested) gene-specific forward primers. Gene-specific PCR was performed using a pair of gene-specific primers (Dataset S6). Both poly(A) tail and gene-specific PCR products were separated on an agarose gel (2%). Poly(A) tail PCR products were also ligated in the pZeroback Blunt vector, and the resulting clones were subjected to Sanger sequencing to determine the actual length of poly(A) tails.

Phalloidin and Hoechst stainings

Embryos were fixed in 4% paraformaldehyde at 4°C overnight and whole-mount stained with rhodamine-labeled (TRITC) phalloidin (Sigma-Aldrich). They were then embbeded in JB-4 resin according to published protocol (15), and 4 μm sections were made and counterstained with Hoechst 33342 (Sigma-Aldrich). Images were acquired using a confocal microscope (Zeiss LSM880), and Z-stack projections were obtained by using the z-projection function.

Immunofluorescence

Embryos were fixed in 4% paraformaldehyde and embedded in paraffin to prepare 4 μm sections. Antigen retrieval was performed by treating sections in 10 mM citrate buffer (pH 6.0) at 100°C (121°C for Pax6 antibody) for 20 minutes. The sections were then treated for immunofluorescence staining and counterstained with DAPI as described (16). Primary antibodies with immunoreactivity in zebrafish include Pax6 (1/100; 901301, Biolegend), AQP0 (1/100; AB3071, Sigma-Aldrich), pH3 (1/300; ab183626, Abcam), and Lamin B1 (1:200; ab16048, Abcam). Alexa Fluor 488 rabbit anti-mouse IgG and goat anti-rabbit IgG (1/500; Interchim) were used as secondary antibodies. Immunofluorescence was analyzed under a confocal microscope (Zeiss LSM880).

Confocal reflection microscopy

Live embryos were embedded in 1% low melting agarose, and reflection images were acquired under a confocal microscope (Zeiss LSM880) using the 405 nm laser at its reflection mode. A total of 10 optical sections were scanned at 3 μm intervals, and they were flattened either by maximum projection or by color-coded projection. The integrated density of the lens region from the maximum projection image was analyzed by Image J software.

BrdU incorporation and apoptosis assays

These were performed as previously described (17). In brief, dechorionated embryos were incubated in Ringer's solution containing 10 mM BrdU (Roche Diagnostics) and 15% dimethylsulfoxide on ice for 15 minutes, briefly washed 3 times with Ringer's solution, and recovered at 28.5°C for 30 minutes. They were fixed in 4% paraformaldehyde at 4°C overnight, and paraffin sections were incubated in anti-BrdU antibody (1/50; sc-32323, Santa Cruz), followed by incubation with Alexa Fluor488 rabbit anti-mouse IgG.

Labeling of apoptotic cells was performed on paraffin sections, using the TUNEL kit according to manufacturer's recommendations (Roche Diagnostics). Positive control was performed by treatment of sections with 3000 UmL^{-1} DNase I (50 mM Tris-HCl, pH 7.5, 1 $mgmL^{-1}$ bovine serum albumin) at 25°C for 10 minutes.

Actinomycin D treatment

WT embryos and *rbm24a* mutants at 33 hpf were dechorionated using 1 $mgmL^{-1}$ pronase, and head regions were dissected in Ringer's solution supplemented with penicillin-streptomycin. The explants

were treated with 0.25% trypsin-EDTA at 37 °C for 15 minutes to increase permeability. Following a brief wash in Ringer's buffer, they were treated with actinomycin D (20 μgmL^{-1}) for different periods.

qRT-PCR

Total RNAs were treated with RNase-free DNase I (Roche Diagnostics). Quantitative analysis of gene expression was performed using Quant qRT-PCR kit (Tiangen), following reverse transcription using oligo-d(T) primer. The $2^{-\Delta\Delta Ct}$ method (18) was employed to estimate relative expression level. Primers used are listed in Dataset S6.

In situ hybridization

The coding regions of different lens-expressed genes were amplified by PCR from embryonic cDNAs, and cloned in pZeroback Blunt vector (Tiangen). DNA templates were PCR amplified and antisense probes were synthesized in the presence of digoxygenin-labeled rNTP mix (Roche Diagnostics). Embryos were fixed in 4% paraformaldehyde at 4°C overnight and stored in methanol. In situ hybridization was performed using published protocol (19). To detect the localization of *rbm24a* expression in the lens after whole-mount in situ hybridization, embryos were embbeded in JB-4 resin and sectioned using an untramicrotome (PowerTome-XL) with a glass knife. The sections were counterstained with eosin Y.

Co-immunoprecipitation

Crosslinked anti-GFP antibody beads were used for immunoprecipitation experiments. Briefly, anti-GFP antibody (0.4 $mgmL^{-1}$) was incubated overnight with protein G Dynabeads at a volume ratio of 3/25. After rinsing in BS_3 binding buffer (20 mM sodium phosphate, pH 8.0), the beads and antibody were crosslinked in 1 mM BS_3 working solution for 30 minutes at room temperature and then quenched in 50 mM Tris-HCl (pH 7.5). They were washed and stored at 4°C in blocking buffer (0.5% bovine serum albumin, 0.02% sodium azide in PBS) before use. Synthetic mRNAs (300 pg) were injected into each 1-cell stage embryo, and about 100 injected embryos were harvested at approximately 10 hpf. Following dechorionation and deyolking, intact cells were collected by centrifugation at 300 *g*, and homogenized in lysis buffer (10 mM Tris HCl, pH 8.0, 150 mM NaCl, 1% NP40, 1 mM EDTA) with protease inhibitors. After saving 30 µL for input control, the lysate was incubated with 25 µL beads overnight in an eppendorf tube under rotation. The beads were rinsed 4 times with lysis buffer, and bound proteins were eluted using Laemmli buffer at 95 °C for 5 minutes and analyzed by Western blot.

Western blot

Zebrafish embryonic proteins were extracted in ice-cold lysis buffer as described (20). The samples were separated by polyacrylamide gel electrophoresis and transferred to nitrocellulose membrane. They were incubated with polyclonal anti-GFP antibody (1/2000; Roche Diagnostics), anti-myc antibody (1/5000; Abcam) or anti-ß-actin antibody (1/5000; Proteintech) at 4°C overnight, followed by horseradish peroxidase conjugated secondary antibody (1/10000, INTERCHIM). Labeled proteins

were detected using the Western-Lightning Plus-ECL substrate (PerkinElmer), and the intensity was analyzed by Lane 1D software.

Mass spectrometry

Head regions were dissected from 110 WT embryos or *rbm24a* mutants at 2 dpf, and were quickly frozen in liquid nitrogen. Following lysate preparation, samples were subjected to in-solution digestion and labeled with Tandem Mass Tags (TMT). Peptide identification and quantification were performed using a liquid chromatography-tandem mass spectrometry (LC-MS/MS). The experiment was independently replicated thrice. Alternatively, proteins from 200 lenses isolated at 2 dpf were resolved by polyacrylamide gel electrophoresis and silver-stained. Protein bands with clear differences between WT embryos and *rbm24a* mutants were excised and subjected to in-gel digestion and peptide extraction. The samples were subjected to mass spectrometry analysis for protein identification.

Real-time imaging

Real-time movies were generated using a stereomicroscope (Leica M165) and the LAS V4.3 software, and edited via Adobe Premiere Pro CC software.

Histology

Embryos were fixed in 4% paraformaldehyde in PBS overnight. They were embedded in JB-4 resin and 4 μm sections were prepared using an untramicrotome (PowerTome-XL) with a glass knife and stained with hematoxylin and eosin Y.

Statistical analyses

All data were collected from at least three independent experiments using different batches of embryos, and representative images were shown. Statistical analysis was performed using unpaired Student's *t*-test and GraphPad Prism 6 software, and *p* values are indicated in the corresponding figures and figure legends.

Data and code availability

Sequencing data that support the findings of this study have been deposited in the Gene Expression Omnibus (GEO) under accession codes GEO136006 and GEO136003. Source data for figures are provided in Dataset S3. All other data supporting the findings are available from the corresponding authors on reasonable request.

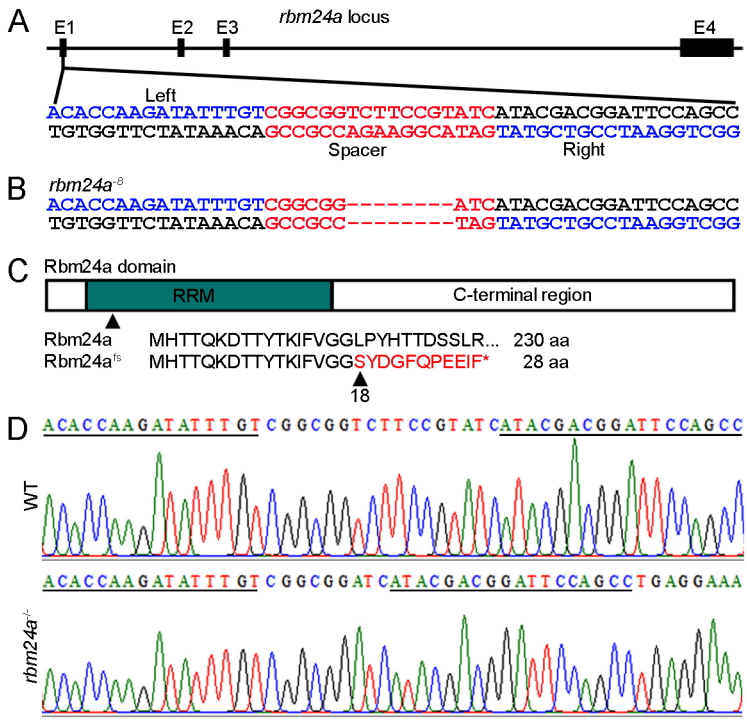

Fig. S1. Generation of zebrafish *rbm24a* mutant line. (*A*) Schema shows the genomic organization of *rbm24a* locus. TALEN recognition sequences within the first exon (E1) are indicated in blue, and the spacer region is shown in red. (*B*) Deletion of 8 nucleotides (dashed lines) in the spacer region. (*C*) Schema of Rbm24a protein domains and alignment of the first 28 amino acids in WT and mutated Rbm24a proteins. The triangles indicate the position where amino acid change occurs. (*D*) Sequencing chromatograms of RT-PCR products show the mutation of *rbm24a* mRNA. TALENs-targeting sequences are underlined.

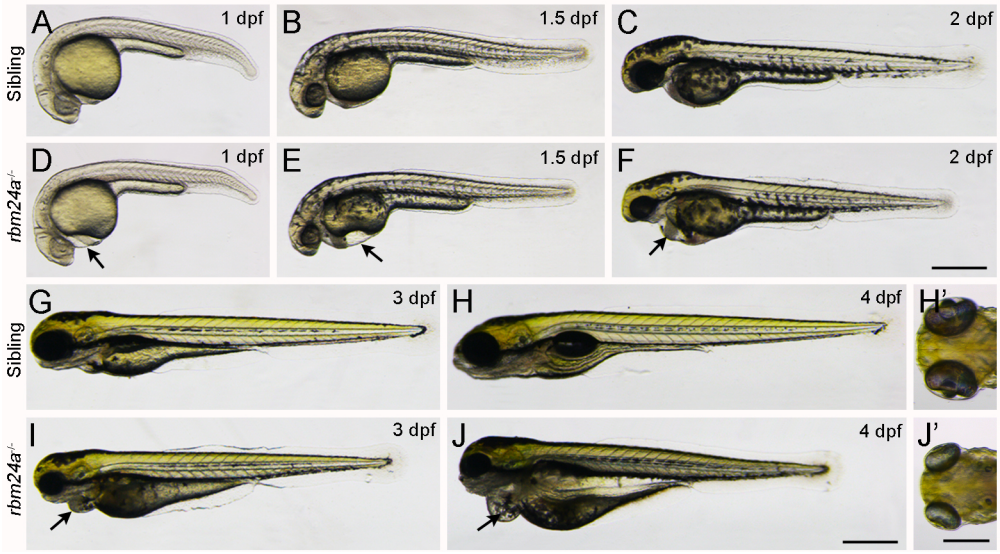

Fig. S2. Phenotypes of *rbm24a* mutants during early development. (*A-C*, *G* and *H*) Live images of WT siblings. Scale bar, 500 μm. (*D-F*, *I* and *J*) Live images of homozygous *rbm24a* mutants show heart edema (arrows) and shortened anteroposterior axis. Scale bar, 500 μm. (*H'* and *J'*) Ventral views show head phenotypes of WT siblings and *rbm24a* mutants at 4 dpf. Note the microcephaly and microphthalmia defects in *rbm24a* mutants. Scale bar, 250 μm.

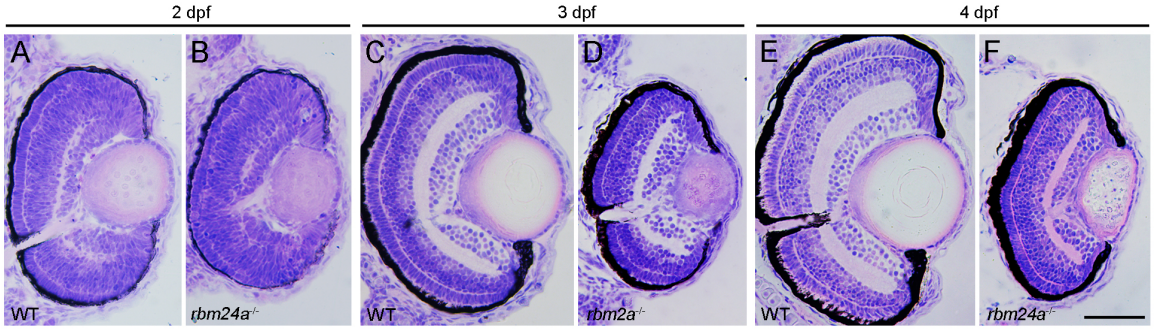

Fig. S3. Defective lens fiber cell denucleation in *rbm24a* mutants. (*A-F*) Hematoxylin and eosin stainings of histological sections at the level of optic nerve compare lens differentiation in WT embryos and *rbm24a* mutants. At 2 dpf, fiber cell nuclei are present in the lens mass of both WT siblings and *rbm24a* mutants. At 3 and 4 dpf, the lens in *rbm24a* mutants still retains fiber cell nuclei and lacks transparency. Note that retinal layers differentiate properly in *rbm24a* mutants despite of strongly reduced eye size. Scale bar, 50 μm.

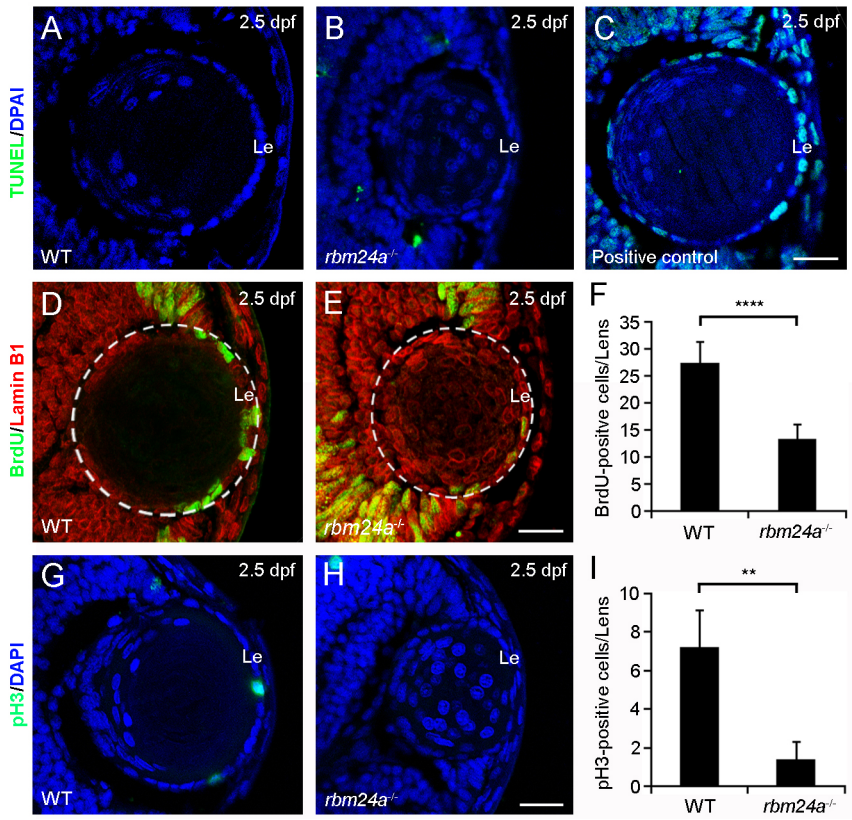

Fig. S4. Defective proliferation of lens epithelial cells in *rbm24a* mutants. (*A*-*C*) TUNEL labeling and DAPI counterstaining of lens sections reveal no differences in cell death within lens epithelium (Le) between WT siblings and *rbm24a* mutants at 2.5 dpf. Scale bar, 20 μm. (*D* and *E*) BrdU labeling compares cell proliferation in lens epithelium between WT siblings and *rbm24a* mutants at 2.5 dpf. The sections were counterstained in red with anti-Lamin B1 antibody to compare fiber cell denucleation in the lens (outline dashed circle) between WT embryos and *rbm24a* mutants. Scale bar, 20 μm. (*F*) Statistical analysis of BrdU-positive cells from 6 independent lenses (****, $P < 0.0001$, Student's *t*-test). (*G* and *H*) Immunofluorescence staining of phospho-Histone H3 (pH3) and DAPI counterstaining in lens sections from WT siblings and *rbm24a* mutants at 2.5 dpf. Scale bar, 20 μm. (*I*) Statistical analysis of pH3-positive cells from 5 independent lenses (**, $P < 0.01$, Student's *t*-test).

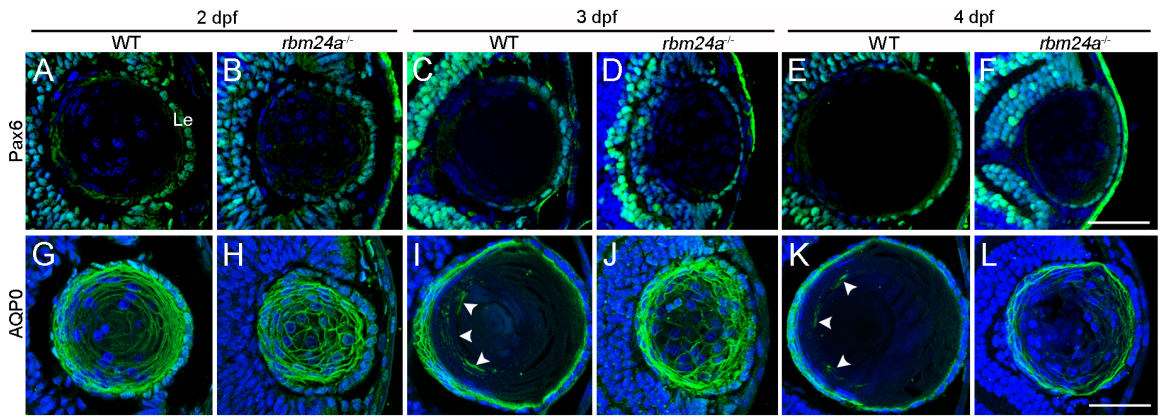

Fig. S5. Defective elongation of lens fiber cells in *rbm24a* mutants. (*A-F*) Immunofluorescence staining and DAPI counterstaining show comparable expression of Pax6 in anterior epithelial cells (Le) between WT siblings and *rbm24a* mutants during lens differentiation. Scale bar, 50 μm. (*G-L*) AQP0 immunofluorescence staining and DAPI counterstaining compare the elongation (arrowheads) of fiber cells between WT siblings and *rbm24a* mutants during lens differentiation. Scale bar: 50 μm.

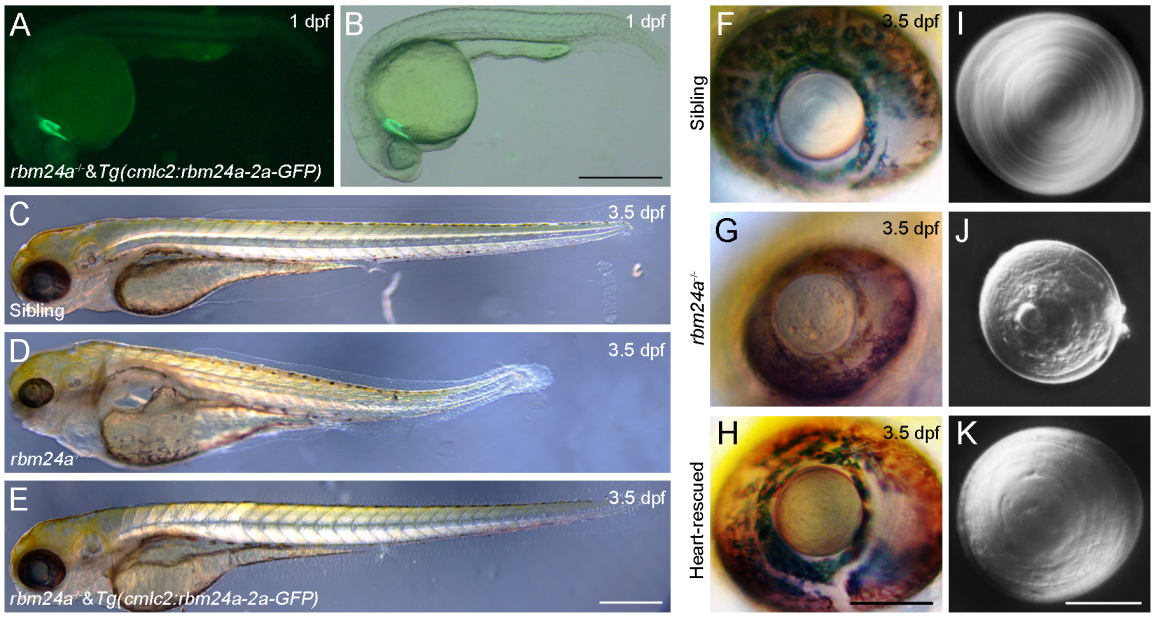

Fig. S6. Presence of cataract phenotype and absence of microphthalmia defects in heart-rescued *rbm24a* mutants. (*A* and *B*) Dark and bright fields show the expression of *Tg(cmlc2-rbm24a-2a-GFP)* transgene in the heart of *rbm24a* mutants at 1 dpf. Scale bar, 500 μm. (*C-E*) Live images of WT siblings, *rbm24a* mutants, and heart-rescued *rbm24a* mutants at 3.5 dpf. Scale bar, 200 μm. (*F-H*) Eye phenotypes in WT siblings, *rbm24a* mutants, and heart-rescued *rbm24a* mutants at 3.5 dpf. (*I-K*) Live images of surgically dissected lenses from WT siblings, *rbm24a* mutants, and heart-rescued *rbm24a* mutants at 3.5 dpf. Scale bar, 50 μm.

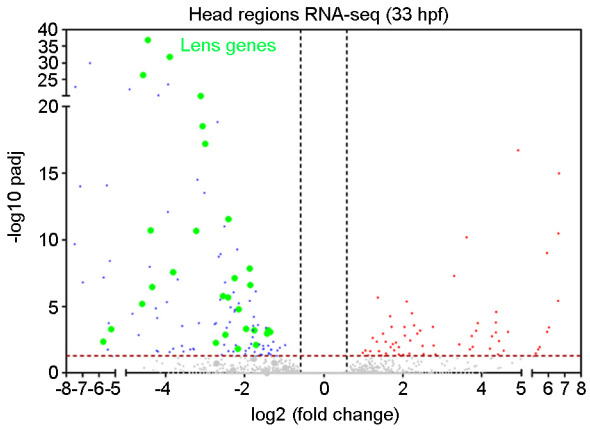

Fig. S7. RNA-seq analysis of Rbm24a-regulated gene expression in the lens. Polyadenylated mRNA samples were prepared from the head regions of WT siblings and *rbm24a* mutants at 33 hpf. Volcano plot shows the down-regulation of lens-related genes coding for crystallins and heat shock proteins in *rbm24a* mutants (green dots).

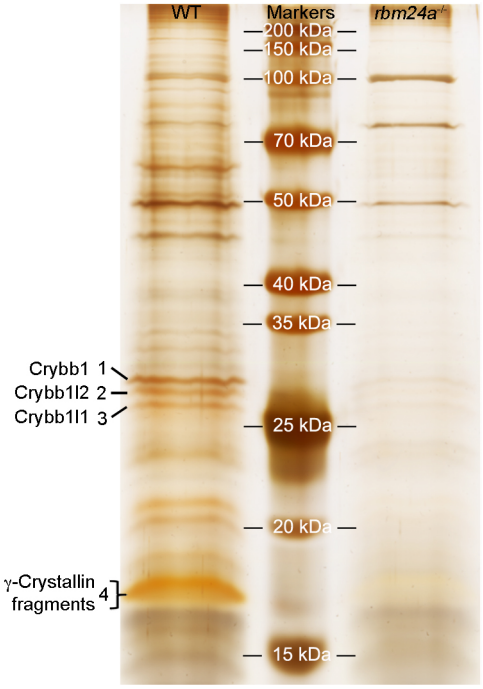

Fig. S8. Reduced accumulation of endogenous crystallin proteins in *rbm24a* mutants. Lenses were dissected from WT siblings and *rbm24a* mutants at 2 dpf, and protein samples were subjected to SDS-PAGE. The gel was silver-stained and slices corresponding to numbered bands were analyzed by mass spectrometry for protein identification.

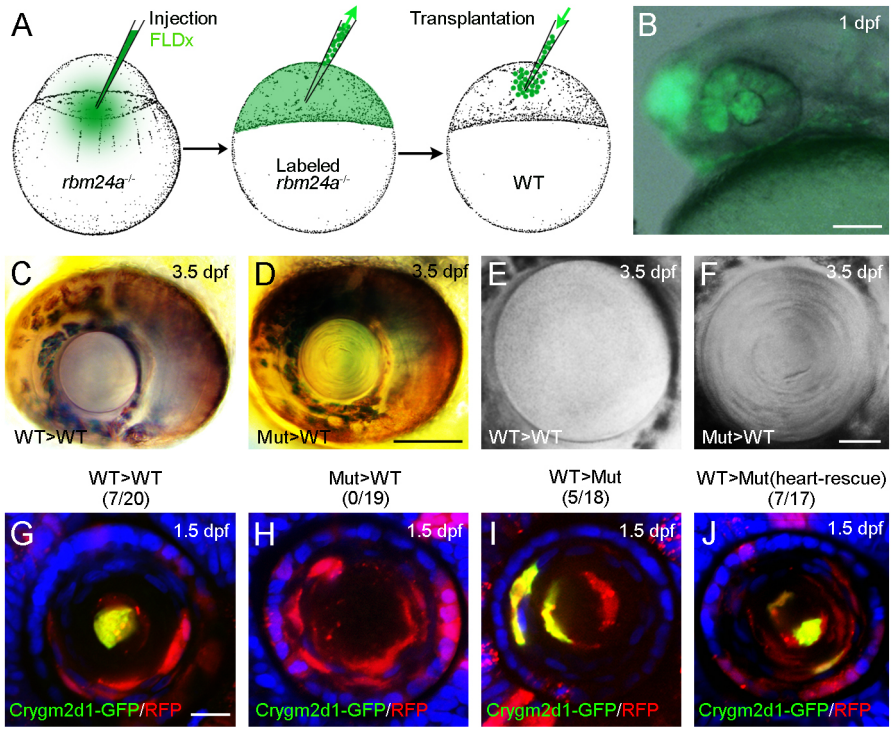

Fig. S9. Cell autonomous effect of *rbm24a* mutation on cataract formation and lens fiber cell differentiation. (*A*) Schema illustrating the transplantation of *rbm24a* mutant cells into WT embryos. (*B*) Identification of chimeric embryos with fluorescent cells in the lens. Scale bar, 200 μm. (*C* and *D*) Eye phenotypes at 3.5 dpf. Scale bar, 100 μm. (*E* and *F*) Lens phenotypes at 3.5 dpf. Scale bar, 25 μm. (*G-J*) Cell transplantation using RFP to label donor cells and the *crygm2d1-GFP* reporter to monitor lens fiber cell differentiation. Donor embryos were injected with mRNA encoding RFP along with the reporter DNA before transplantation. In contrast to WT cells, transplanted *rbm24a* mutant cells do not express the fusion protein in the WT recipient lens, while transplanted WT cells differentiate autonomously in the lens of *rbm24a* mutants, and heart-rescued *rbm24a* mutants. Numbers in parentheses represent total lenses with RFP and GFP double-labeled cells relative to total lenses with only RFP-labeled cells. Due to the extremely mosaic distribution of the injected reporter DNA, GFP signal is not present in all RFP-labeled cells. Scale bar: 25 μm.

Movie S1 (separate file). Real-time movies show heart beating and blood circulation in a WT embryo and an *rbm24a* mutant at 3 dpf. In the mutant, blood is transported back and forth between the ventricle and atrium, indicating defective atrial valve and absence of blood flow.

Movie S2 (separate file). Real-time movie shows fused circulatory systems in heterotypically parabiosed embryos at 3.5 dpf. Blood circulation can be seen in the eyes of both partners.

Movie S3 (separate file). Real-time movies show the prey capture behavior of WT and chimeric larvae. The wild-type larva focuses its eyes on free-swimming paramecia, followed by a predatory action. The chimera containing bulk of *rbm24a* mutant cells in the WT recipient lens fails to detect the presence of paramecia. Both larvae were at 5 dpf.

Dataset S1 (separate file). Comparison of Rbm24-regulated muscle-specific alternative splicing (AS) events between mouse and zebrafish.

Dataset S2 (separate file). Identification of alternative splicing events in WT embryos and *rbm24a* mutants.

Dataset S3 (separate file). Source data for figures.

Dataset S4 (separate file). Head region proteomics analyzed by mass spectrometry, corresponding to Fig. 7*G*.

Dataset S5 (separate file). Characterization of protein bands by mass spectrometry, corresponding to Fig. S8. Identified proteins are ordered by their abundance, which is defined as the ratio of peptide counts divided by the molecular weight of the protein. The most abundant proteins are highlighted in yellow.

Dataset S6 (separate file). List of primers used in this study.

SI References

1. T. Cermak *et al*., Efficient design and assembly of custom TALEN and other TAL effector-based constructs for DNA targeting. *Nucleic. Acids Res*. **39**, e82 (2011).
2. Y. Lei *et al*., Efficient targeted gene disruption in Xenopus embryos using engineered transcription activator-like effector nucleases (TALENs). *Proc. Natl. Acad. Sci. U. S. A*. **109**, 17484-17489 (2012).
3. Y.-Y. Xing *et al*., Mutational analysis of dishevelled genes in zebrafish reveals distinct functions in embryonic patterning and gastrulation cell movements. *PLoS Genet.* **14**, e1007551 (2018).
4. A. Urasaki, G. Morvan, K. Kawakami, Functional dissection of the Tol2 transposable element identified the minimal cis-sequence and a highly repetitive sequence in the subterminal region essential for transposition. *Genetics* **174**, 639-649 (2016).
5. C. Huang, C.-T. Tu, C.-D. Hsiao, F.-J. Hsieh, H.-J. Tsai, Germ-line transmission of a myocardium-specific GFP transgene reveals critical regulatory elements in the cardiac myosin light chain 2 promoter of zebrafish. *Dev. Dyn*. **228**, 30-40 (2003).
6. X.-N. Cheng *et al*., Leucine repeat adaptor protein 1 interacts with Dishevelled to regulate gastrulation cell movements in zebrafish. *Nat. Commun.* **8**, 1353 (2017).
7. M. Shao *et al*., Vegetally localised Vrtn functions as a novel repressor to modulate *bmp2b* transcription during dorsoventral patterning in zebrafish. *Development* **144**, 3361-3374 (2017).
8. M. Shao, X.-N. Cheng, Y.-Y. Liu, J.-T. Li, D.-L. Shi, Transplantation of zebrafish cells by conventional pneumatic microinjector. *Zebrafish* **15**, 73-76 (2018).
9. S. Anders, P.-T. Pyl, W. Huber, HTSeq--a Python framework to work with high-throughput sequencing data. *Bioinformatics* **31**, 166-169 (2015).
10. M. Martin, Cutadapt removes adapter sequences from high-throughput sequencing reads. *EMBnet.journal* **17**, 10-12 (2011).
11. M.-I. Love, W. Huber, S. Anders, Moderated estimation of fold change and dispersion for RNA-seq data with DESeq2. *Genome Biol*. **15**, 550 (2014).
12. M.-D. Robinson, D.-J. McCarthy, G.-K. Smyth, edgeR: a Bioconductor package for differential expression analysis of digital gene expression data. *Bioinformatics* **26**, 139-140 (2010).
13. L. Florea, L. Song, S.-L. Salzberg, Thousands of exon skipping events differentiate among splicing patterns in sixteen human tissues. *F1000Research* **2**, 188 (2013).
14. C. Trapnell *et al*., Differential gene and transcript expression analysis of RNA-seq experiments with TopHat and Cufflinks. *Nat. Protoc*. **7**, 562-578 (2013).
15. J. Sullivan-Brown, M.-E. Bisher, R.-D. Burdine, Embedding, serial sectioning and staining of zebrafish embryos using JB-4 resin. *Nat. Protoc*. **6**, 46-55 (2011).
16. R. Grifone, A. Saquet, Z.-G. Xu, D.-L. Shi, Expression patterns of Rbm24 in lens, nasal epithelium, and inner ear during mouse embryonic development. *Dev. Dyn.* **247**, 1160-1169 (2018).

17. X.-N. Cheng, M. Shao, D.-L. Shi, Mutation of frizzled8a delays neural retinal cell differentiation and results in microphthalmia in zebrafish. *Int. J. Dev. Biol*. **62**, 285-291 (2018).
18. K.-J. Livak, T.-D. Schmittgen, Analysis of relative gene expression data using real-time quantitative PCR and the 2(-Delta Delta C(T)) Method. *Methods* **25**, 402-408 (2001).
19. M. Westerfield, “The zebrafish book: a guide for the laboratory use of zebrafish (Danio rerio)”, 5th Edition (University of Oregon Press, 2007).
20. X.-N. Cheng, M. Shao, D.-L. Shi, Collagen triple helix repeat containing 1a (Cthrc1a) regulates cell adhesion and migration during gastrulation in zebrafish. *Exp. Cell Res*. **381**, 112-120 (2019).